THE JOURNAL OF PHYSICAL CHEMISTRY B

Article

pubs.acs.org/JPCB

Identification of 13- and 14-Coordinated Structures of First Hydrated Shell of $[AuCl_4]^-$ Acid Aqueous Solution by Combination of MD and XANES

Qing Ye,[†] Jing Zhou,[†] Ting Zhao,[†] Haifeng Zhao,[†] Wangsheng Chu,[‡,†] Zhengxu Sheng,[‡] Xing Chen,*[,‡] Augusto Marcelli,[§,‡] Yi Luo,*[,∥] and Ziyu Wu*[,†,‡]

[†]Beijing Synchrotron Radiation Facility, Institute of High Energy Physics, CAS, 100049 Beijing, China

[‡]National Synchrotron Radiation Lab, University of Science and Technology of China, 230029 Hefei Anhui, China

[§]Istituto Nazionale di Fisica Nucleare, Laboratori Nazionali di Frascati, 00044 Frascati, Italy

[∥]Hefei National Laboratory for Physical Sciences at Microscale, University of Science and Technology of China, 30029 Hefei Anhui, China

Supporting Information

ABSTRACT: Molecular dynamics simulations combined with multiple scatting X-ray absorption spectral calculations have been employed to study the local geometry of an $[AuCl_4]^-$ cluster in acid aqueous solution. It is found that the previously assumed simple octahedral structure with two H atoms located in the axial position of the $[AuCl_4]^-$ plane fails to correctly reproduce the experimental X-ray absorption spectra. Molecular dynamics simulations have revealed a very complicated first hydrated water shell that mainly consists of 13 or 14 ligand water molecules. In general, the first hydrated water molecules are located in two orthogonal quasi-elliptic surfaces around $[AuCl_4]^-$ cluster. The water molecules' configuration in the first hydrated shell is further confirmed by the X-ray absorption spectral analysis, which gives a good agreement with the experiment when the 13-hydrated and 14-hydrated complexes are evenly mixed. It shows the power of the combined molecular dynamics simulations and spectra calculations in determining the local structure of molecular ligands around the metal center.

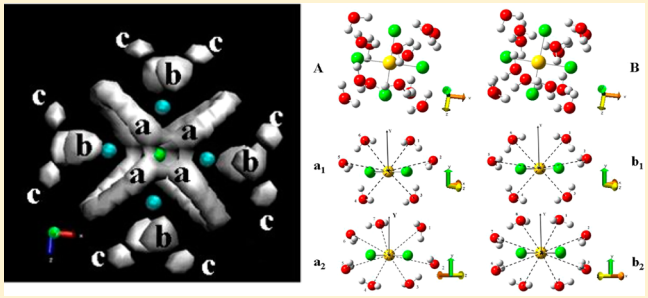

1. INTRODUCTION

The aqueous solution of $[AuCl_4]^-$ is an important substance with wide applications. It can be used as a reagent to reduce gold nanoparticles and colloidal gold,[1−4] as a dopant in polymer thin-film transistors to enhance the electrical properties[5] and a compound for sonoluminescence and sonochemistry applications.[6] How the water molecules are coordinated around the $[AuCl_4]^-$ is a challenging problem owing to the relatively weak interaction between them. A four-coordinated square planar structure with an Au−Cl distance of 2.28−2.29 Å in the $HAuCl_4$ aqueous solution has been identified, and structural changes of the $[AuCl_n(OH)_{4-n}]^-$ vs pH have been also outlined by extended X-ray absorption fine structure (EXAFS).[7,8] Raman investigations pointed out that, in acidic aqueous solutions, the square-planar geometry seems to be stable in the temperature range 25−100 °C.[9] Very recently, the reaction of $HAuCl_4$ with sodium hydroxide and glucose has been studied by the quick extended X-ray absorption fine structure (QEXAFS), and it is suggested that the hydrogen atoms (maybe H atoms in water molecular or H^+ ions) are probably present in the axial position of the $[AuCl_4]^-$ plane in a distance of 1.5 Å.[10] Intuitively, one might suspect that these proposed structures are somewhat unrealistic based on the fact that the $[AuCl_4]^-$ cluster has a relative diffuse charge distribution and weak attraction to water molecules. One would expect to obtain a more complicated and loosely bounded hydrated shell around the $[AuCl_4]^-$ cluster.

Here, we carry out molecular dynamics simulations to examine the local structure of water molecules around the $[AuCl_4]^-$ cluster in aqueous solution, and the obtained structures are verified by comparing the calculated and experimental X-ray absorption near edge structure (XANES). For the calculations, a large number of configurations from MD trajectory have been considered to obtain the statistically meaningful results. This theoretical scheme has been successfully applied to study the influence of structure disorder on the XANES and resolved local structure of several important aqueous single metal ion solutions[11−15] and even Fe ion in protein.[16] We have found that the local geometry of the $[AuCl_4]^-$ cluster can be characterized by a loose, complex, and

Received: March 20, 2012
Revised: June 8, 2012
Published: June 11, 2012

structure-changeable hydrated shell with high coordination numbers, in contrast to the simple ones assumed in previous studies. The water molecules in the first hydrated shell are preferably located in two orthogonal quasi-elliptic surfaces and are frequently switched in between coordination numbers of 13 and 14. The calculated spectrum based on the structures obtained from MD simulations is in good agreement with the experiment, verifying the reliability of the proposed water hydrated configuration for the first hydrated shell of the $[AuCl_4]^-$ cluster.

2. EXPERIMENTAL SECTION

2.1. Sample Preparation. Analytical grade of tetra-aquo chloroauric acid ($HAuCl_4{\cdot}4H_2O$) was obtained from Beijing chemicals company. The $HAuCl_4$ was dissolved in water to obtain a 0.25 M $HAuCl_4$ aqueous solution.

2.2. X-ray Absorption Characterization. Au L_3-edge X-ray absorption spectroscopy (XAS) was collected at the XAFS station of the Beijing Synchrotron Radiation Facility (BSRF) with the storage ring working at 2.2 GeV with an average electron current of 80 mA. The X-ray beam was monochromatized by a double-crystal Si (111) monochromator characterized at the energy resolution $\Delta E/E \approx 3 \times 10^{-4}$. The energy was calibrated using a gold metal foil. Solutions were measured with a Teflon cell and the thickness of the solution was adjusted optimizing the absorption thickness $\Delta\mu d \approx 1$. $\Delta\mu$ is the absorption edge jump, and d is the thickness of the solution inside the cell. XAS at the Au-L_3 edge were recorded in transmission mode at room temperature, and both incident and transmission intensities were detected using two ionization chambers placed before and after the liquid cell.

2.3. XANES Analysis. XANES calculations based on a self-consistent multiple-scattering (MS) method were carried out using the FEFF8.2 code.[17] For the exchange correlation part of the potential, we chose the Hedin–Lundqvist (HL) model. Spectra were first background subtracted by fitting the pre-edge using a least-squares method, and then, all spectra were normalized to one at energies far from the edge.

2.4. Molecular Dynamic (MD) Simulations. The simulation was carried out using a GROMACS package, version 4.0.7,[18] modified to include our self-constructed interaction model. One square planar $[AuCl_4]^-$ cluster with Au–Cl bond length of 2.28 Å and 503 SPC/E water molecules were confined in a cubic box of volume ≈ 15.625 nm^3 with a periodic boundary condition. The system has been simulated in a NVT ensemble at $T = 300$ K with the Berendsen temperature coupling and a coupling constant of 0.1 ps.[19] A cutoff of 10 Å was used to deal with nonbonded interactions and the particle mesh Ewald method[20,21] to take care of long-range electrostatic effects. An homogeneous background charge was used to compensate for the presence of the $[AuCl_4]^-$ cluster.[22] The simulation lasts for 105 ns with steps of 1 fs, while the actual configuration has been stored after each picosecond.

3. RESULTS AND DISCUSSION

3.1. Simple Structure. Normalized Au-L_3 edge XANES as well as calculated spectra from three proposed structures in ref 10 are shown in Figure 1. The structures are characterized by an Au–Cl bond length of 2.29 Å and two H atoms locate at the axial orientation with an Au–H distance of 1.5 Å, while the water molecules are represented with the SPC/E model, we can see that the features B and C both have a red shift when the

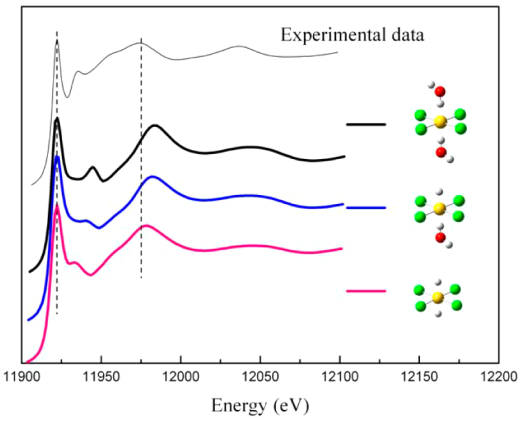

Figure 1. Comparison between the experimental Au-L_3 XANES and calculated spectra from the proposed structures.

employed structure has two, one, and zero water molecules, but the fact that even the spectrum calculated from the cluster only has two H atoms shows poor agreement with the experimental data and indicates that the axial ligand structure is unreliable.

3.2. Force Fields. For the sake of accuracy, it is necessary to construct a reliable potential model to describe the interaction among the $[AuCl_4]^-$ cluster and water molecules. To describe the $[AuCl_4]^-$–water system, we have chosen the so-called effective pair potential that exhibits high-level performances for transition elements in ion–water systems.[23−25] The potential energy surface (PES) of the $[AuCl_4]^-$–H_2O was scanned, and the restricted open-shell Hartree–Fock (ROHF)[26] coupling with a conductor-like polarizable continuum model (CPCM) was employed to simulate the effect of the bulk solvent condition during the scan. The CEP-121G basis set and corresponding core pseudopotential was used for Au,[27−29] the STO-3G basis set for Cl,[30,31] and the cc-PVTZ basis set for the water molecule.[32] The PES generated from ab initio calculations has been fit with the following pair potential:

$$U = \sum_{i=\mathrm{Au,Cl};\, j=\mathrm{O}} \frac{q_i q_j}{\varepsilon r_{ij}} + \frac{A_{ij}}{r_{ij}^{4}} + \frac{B_{ij}}{r_{ij}^{6}} + \frac{C_{ij}}{r_{ij}^{8}} + \frac{D_{ij}}{r_{ij}^{12}} + E_{ij}\exp(-F_{ij}r_{ij}) + \sum_{m=\mathrm{Au,Cl};\, n=\mathrm{H}} \frac{q_m q_n}{\varepsilon r_{mn}} + \frac{A_{mn}}{r_{mn}^{4}} + \frac{B_{mn}}{r_{mn}^{6}} + \frac{C_{mn}}{r_{mn}^{8}} + \frac{D_{mn}}{r_{mn}^{12}}$$

where q_i refers to the electrostatic charge of the atom i, ε to the permittivity of vacuum, and r_{ij} to the distance between atoms i and j. A_{ij}, ..., F_{ij} and A_{mn}, ..., D_{mn} are the fit parameters. The universal global optimization (UGO) algorithm was used to carry out the fit, and the root mean square error (rmse) value achieved is 3.854 kcal/mol/nm^3. The fit parameters are summarized in Table 1. (For a detailed introduction about basis set, PES scan, fit procedure, charge determination, and parameters choice in the CPCM model, please see the Supporting Information). A frequency analysis of a bare $[AuCl_4]^-$ cluster coupled with the CPCM model has been also carried out to construct the harmonic vibration models of bonds, angles, and the dihedral inside the $[AuCl_4]^-$ cluster. In this framework, we obtained a Hessian matrix, which holds the second partial derivatives of the potential V with respect to atomic displacements in Cartesian coordinates. Its matrix element is

dx.doi.org/10.1021/jp3026623 | J. Phys. Chem. B 2012, 116, 7866–7873

Table 1. Best-Fit Parameters of the $[AuCl_4]^-$−Water Effective Pair Potential

A_{Au-O}	B_{Au-O}	C_{Au-O}	D_{Au-O}	E_{Au-O}	F_{Au-O}	A_{Au-H}
4.4935×10^{-5}	2.2085×10^{-1}	-2.0876×10^{-2}	6.3601×10^{-6}	1.0981×10^{7}	40.3349	-2.1159×10^{-1}
B_{Au-H}	C_{Au-H}	D_{Au-H}	A_{Cl-O}	B_{Cl-O}	C_{Cl-O}	D_{Cl-O}
1.6365×10^{-2}	-2.4614×10^{-4}	1.7180×10^{-8}	7.9171×10^{-1}	-3.5028×10^{-1}	1.1773×10^{-2}	-3.7968×10^{-6}
E_{Cl-O}	F_{Cl-O}	A_{Cl-H}	B_{Cl-H}	C_{Cl-H}	D_{Cl-H}	
9.8420×10^{4}	20.8785	1.7744×10^{-2}	1.0834×10^{-2}	3.7536×10^{-4}	-3.1104×10^{-8}	

$$f_{ij} = \left(\frac{\partial^2 V}{\partial q_i \partial q_j}\right)_0$$

where q_i refers to the mass weighted Cartesian coordinates. With $(...)_0$, we point out that derivatives are taken at the equilibrium positions of the atoms, and all first derivatives are zero. More details about the frequency analysis and the Hessian matrix are available in ref 33. The matrix is then transformed in internal coordinates so that the force constants can be derived from the corresponding elements of the matrix. The calculated force constants are summarized in Table 2. The effective pair potential and the intramolecular harmonic vibration models obtained were later introduced in GROMACS to carry out the MD simulation.

Table 2. Force Constants for Bonds and Angles of the $[AuCl_4]^-$ Cluster

Au−Cl bond force constant	Cl−Au−Cl angle force constant (90°)	Cl−Au−Cl angle force constant (180°)	Cl−Au−Cl−Cl dihedral angle force constant
2.0168×10^5 kJ/mol/nm^2	1498.14 kJ/mol/rad^2	749.07 kJ/mol/rad^2	388.29 kJ/mol/rad^2

3.3. Global Structures. In order to give a first intuitive layout of the hydrated shell around the $[AuCl_4]^-$ cluster, the particle-number-density isosurface of oxygen atoms characterized by a C_{4h} symmetry as well as the 2D oxygen atoms density maps projected along the *Y*-axis and the angle bisector of the *X*- and *Z*-axes are shown in Figure 2. The oxygen atoms distribution in the elliptical-shaped volume is clearly not uniform, and oxygens do not prefer localization near the *Y*-axis and the $[AuCl_4]^-$ surface (Figure 2c). According to the Au−O distance, water molecules fall in three well-defined sets: *a*, *b*, and *c* (Figure 2a). The nearest area to the $[AuCl_4]^-$ cluster, identified as *a*, consists of two orthogonal elliptical areas, other water molecules fall in the *b* and *c* areas located far from the $[AuCl_4]^-$ cluster. Water molecules outside these regions can be considered as bulk water.

To characterize the structural arrangement of water molecules, we present the theoretical Au−O radial distribution function g_{Au-O} calculated from MD simulated trajectory (Figure 3a). The comparison with similar radial distribution of transition metal ions such as Hg^{2+}, Cd^{2+}, and Zn^{2+}[34−36] points out that g_{Au-O} has a relative complicated hydrated structure with two sharp peaks labeled C and D located at about 3.96 Å and 5.02 Å and two shoulders labeled A and B before the peak C. The minimum between peak C and D locates at about 4.34 Å; therefore, we set 4.34 Å as the cutoff to separate the first and second hydration shell. Moreover, looking at Figure 3b, we have to underline that the coordination number of the first shell changes continuously, mainly switching between 13 and 14 coordination, together with the g_{Au-O} value of 0.923 at 4.34 Å, a relatively far distance from baseline, pointing out an instable nature of the first hydrated shell and a fast intershell water molecule exchange process.

3.4. First Hydrated Shell. In our MD simulation, we saved the configurations along the MD trajectory from 10 to 105 ns every picosecond. Among the 95 000 configurations we obtained, 54 709 and 38 910 configurations belong to 14-hydrated and 13-hydrated complexes, respectively. The remaining 1381 configurations involving 11-, 12-, and 15-hydrated complexes accounts for only ∼1%, so that they were neglected in the following discussion. We have to underline also that the longest lifetimes associated to $[AuCl_4]^-(H_2O)_{13}$ and $[AuCl_4]^-(H_2O)_{14}$ clusters were 92 and 125 ps, respectively, much shorter than those of other transition metal ions hydrated clusters, such as $Cd^{2+}(H_2O)_6$ with 2297 ps and $Cd^{2+}(H_2O)_7$

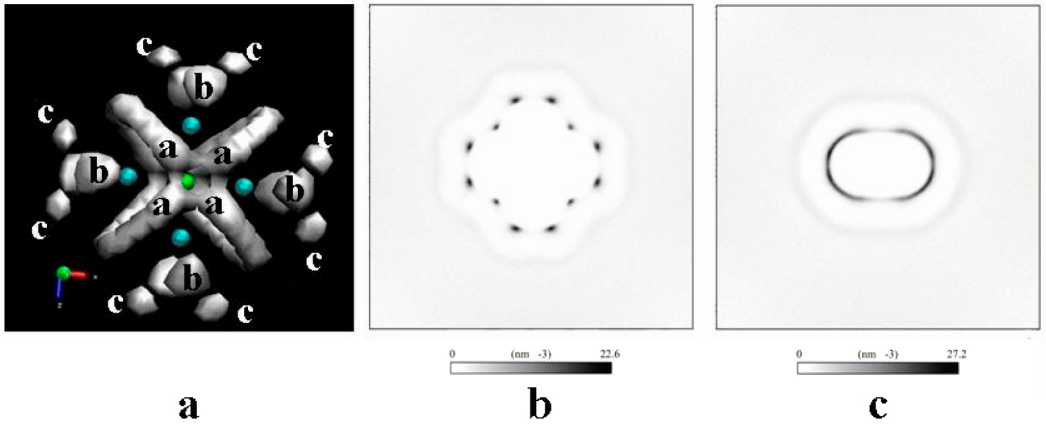

Figure 2. (a) Particle-number-density isosurface of oxygen atoms around the $[AuCl_4]^-$ cluster; (b) 2D density map of oxygen atoms with a projective orientation along the *Y*-axis; and (c) the angular bisector between the *X*- and *Z*-axes.

dx.doi.org/10.1021/jp3026623 | J. Phys. Chem. B 2012, 116, 7866−7873

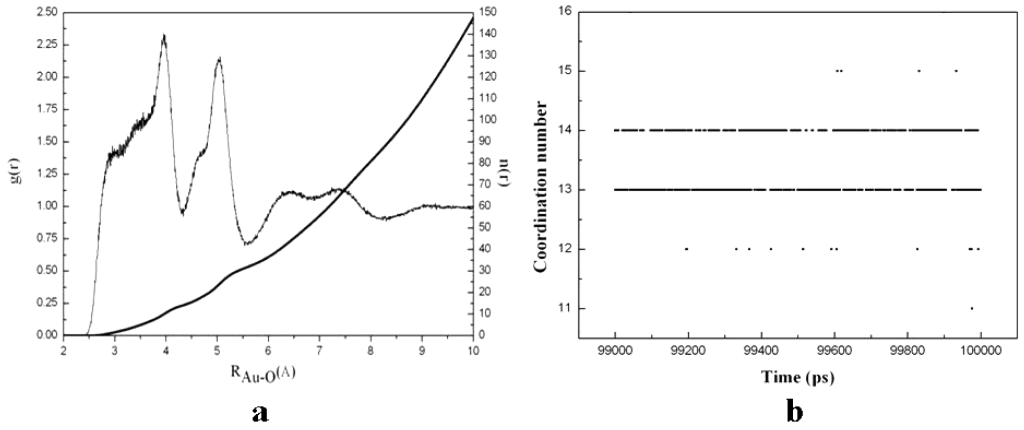

Figure 3. (a) Au−O $g(r)$s calculated on the total trajectories obtained from the MD simulation with the corresponding running integration number and (b) variation of coordination number of the first hydrated shell vs time.

with 1048 ps.[15] Data suggest that the $[AuCl_4]^-$−$(H_2O)_n$ system has a relatively instable hydrated structure and that the coordination number of the first hydrated changes frequently.

To get a deeper insight into the structure of the $[AuCl_4]^-$−$(H_2O)_n$ complex, we analyzed independently MD configurations in which either 13- or 14-hydrated species were present. The corresponding g_{Au-O} shown in Figure 4 points out

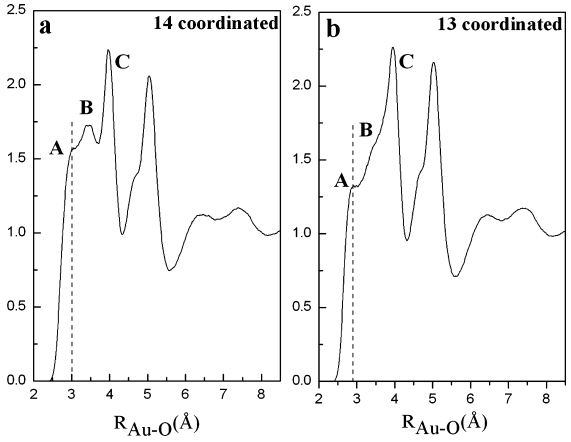

Figure 4. Au−O $g(r)$s calculated from (a) 14-hydrated and (b) 13-hydrated complexes.

clearly that the distribution functions are almost the same for Au−O distances > 4.34 Å, e.g., the water arrangements in the second and higher hydration shell are almost coincident. In other words, differences in the calculations are mainly concentrated in the first hydrated shell. To describe it in more detail, we performed the energy-minimization of both 13- and 14-hydrated configurations, shown in Figure 5. The first-hydrated water molecules in the 13-hydrated complex fall in two orthogonal elliptical areas containing 6 (Figure $5a_1$) and 7 water molecules (Figure $5a_2$), respectively. Instead, in the 14-hydrated complex, the two elliptical areas contain 6 (Figure $5b_1$) and 8 (Figure $5b_2$) water molecules. By combining Figures 4 and 5, we may attribute signal A to the atoms 3, 4, and 7 in Figure $5a_2$ (for 13-hydrated species) and atoma 1, 4, 5, and 8 in Figure $5b_2$ (for 14-hydrated species); signal B to atom 1, 3, 4, and 6 in Figure $5a_1$ and b_1 for both species as well as atom 1 in Figure $5a_2$; signal C can be attributed to other atoms. Meanwhile, the relative intense peak of B in 14-hydrated

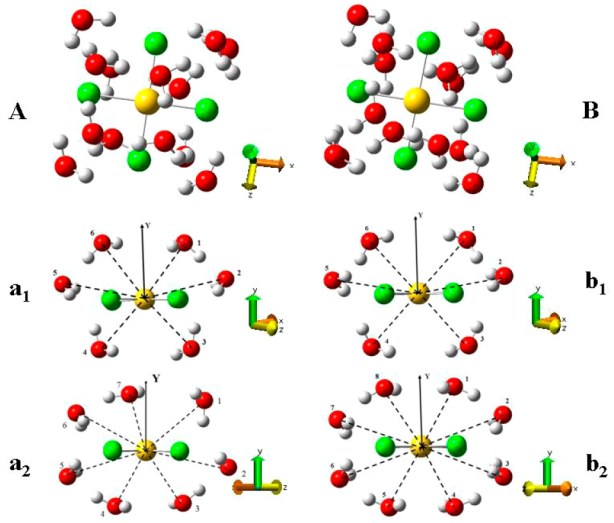

Figure 5. Energy-minimization configurations for (a) 13-hydrated and (b) 14-hydrated complexes.

indicates that the positions of corresponding atoms are relatively stable as compared to the counterpart in 13-hydrated species.

Although the radial distribution function g_{Au-O} is fundamental to reconstruct the cluster, alone it is not sufficient to achieve a detailed and complete picture of the water molecules arrangement around the $[AuCl_4]^-$ cluster. In order to extract additional information about the hydrated structure, we plot in Figure 6 the two angular distribution functions (ADF) of θ and φ of both 13-hydrated and 14-hydrated complexes. Here, θ is defined as the angle between the Au−O vector and the Y-axis, while φ is the angle between the Au−O vector and the water dipole moment. The ADF of θ is shown in Figure 6a. Although the number of configurations we used for the calculation is not large enough to describe a completely symmetric function for both hydrated complexes around 90°, useful structural information can be still obtained. When looking at the shape, we recognized that water molecules do not prefer lying in the $[AuCl_4]^-$ plane or in a plane perpendicular to it, i.e., corresponding to the θ values 0° and 90°. At the same time, both ADFs of the 13- and 14-hydrated complexes exhibit several broad peaks that point out the presence of a disordered water arrangement around the $[AuCl_4]^-$ cluster, a result

dx.doi.org/10.1021/jp3026623 | J. Phys. Chem. B 2012, 116, 7866−7873

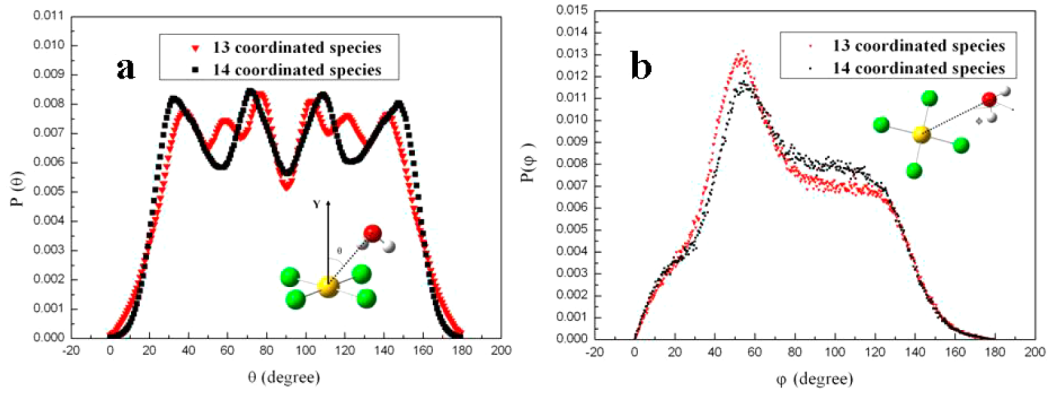

Figure 6. ADF of (a) angular θ and (b) angular φ for 13-hydrated complexes (red) and 14-hydrated complexes (black).

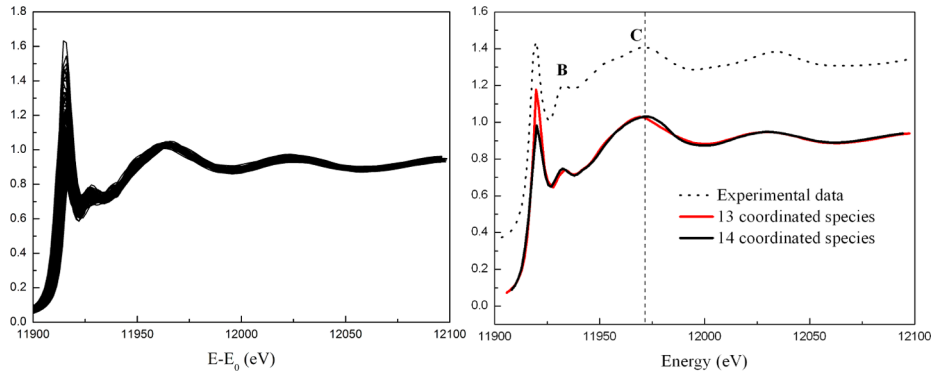

Figure 7. (a) Several spectra calculated from different configurations in MD trajectory. (b) Comparison between experimental data and averaged XANES 13-hydrated (red) and 14-hydrated (black) complexes.

consistent with the RDF analysis. Looking at the ADF of the angle φ (Figure 6b) the preferred orientation of the water dipole moment is neither oriented toward nor opposed to the Au atom, i.e., corresponding to the φ values of 0° and 180°. If compared with some bare transition-metal ions such as zinc(II) and nickel(II), in this case, the broad distribution of φ points out that those water molecules are relatively free to rotate.[23]

It is noted that our obtained 13- and 14-coordinated first hydrated structures are complicated as compared with that in metal ion aqueous solutions, which often adopt an octahedral hydrated structure with two ligands located in the axial orentation.[37,38] To understand the rare hydrated structure $[AuCl_4]^-$ adopts, we may underline that the $[AuCl_4]^-$ cluster is characterized by a more diffuse electron distribution than bare ions; therefore, if compared with Hg^{2+} or Cd^{2+} ions, it exhibits a reduced attraction to a water molecule. Actually, according to our ab initio calculation, the minimum of the $[AuCl_4]^-$–H_2O PES is −122.40 kJ/mol, about two times higher than the PES of the Cd^{2+}–H_2O (−232.60 kJ/mol).[15] During the PES scan, we indeed found a local energy minimum position at the axial orientation of the $[AuCl_4]^-$ cluster, but in the aqueous solution, all the water molecules around axial have a tendency to locate at the energy minimum position, while these water molecules reject each other when they get too close. So the competitive result is that no water molecule locates at the axial position, but they distribute around the axial position. However, for the metal ion aqueous solution, since there is a relatively strong constraint effect of metal ion to water molecule, the pre-energy-minimum-position-located water molecule is relatively difficult to be pushed away by other approaching water molecules. Generally speaking, the relatively weak attraction of the $[AuCl_4]^-$ cluster to water molecules is the main reason to induce a loose, structure changeable, and complex hydrated structure.

Moreover, as discussed above, from the MD simulation, the detected amount of 13- and 14-hydrated complexes are 40.96% and 57.59%, respectively. However, different water models show different dynamic behaviors.[14,39] As an example, compared to models such as ST2,[39] ST4,[40] and TIP5,[41] the SPC/E water model used in our simulation exhibits reduced water mobility. Therefore, the relative ratio obtained from simulations has to be carefully considered. However, rather than investigating the effect of different water models on the relative ratio of hydrated complexes, we are more interested in building a realistic hydrated structure and recognizing the distribution of different complexes of the $[AuCl_4]^-$–water system. As mentioned before, XANES is really sensitive to the geometrical environment around the photoabsorber, and a quantitative analysis of XANES data could provide an answer for the hydration structure of the $[AuCl_4]^-$ cluster. By using the structural information obtained from MD simulation, we analyzed XANES spectra in order to reproduce XANES features.

3.5. Simulations of XANES. As underlined above, the disorder associated to the oscillations among different configurations rules out the occurrence of a single representative configuration. As a consequence, any single configuration is not representative of all the configurations occurring in the $[AuCl_4]^-$ aqueous solution. A demonstration of the structural disorder contribution on the XANES spectra is given in Figure 7a from which we can obtain a general impression of the oscillation of the XANES signal among different configurations;

dx.doi.org/10.1021/jp3026623 | J. Phys. Chem. B 2012, 116, 7866–7873

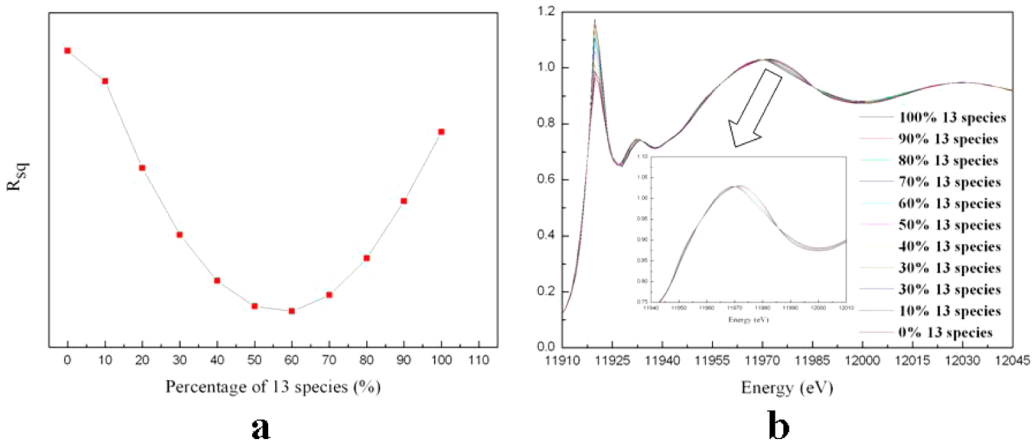

Figure 8. (a) Goodness-of-fit (R_{sq}) varies with the percentage of 13-hydated complexes. (b) Averaged theoretical XANES calculated with different amounts of the two coordinated species.

the oscillation spreads over the whole range of XANES, while mainly locating at the absorption edge, feature B, and a relatively weak oscillation, on feature C and higher energy. To get a deeper understanding about the influence of the disorder effect on XANES, we show here two movies in the Supporting Information. In the Movie 1, we keep the structure of the $[AuCl_4]^-$ cluster unaltered while changing water molecules around the $[AuCl_4]^-$ cluster consistently along the MD trajectory (a fragment from 57 792 to 57 888 ps), while in Movie 2, we freeze the position of water molecules, while changing the Au−Cl bond length of the cluster. By looking at these movies, we may split the structural disorder contribution on the XANES spectra in two components. The first component comes from the high mobility of water molecules that modifies spectra from the absorption edge (11 898.6 eV) up to about 12 050.0 eV. The most evident changes affect the white line intensity, the shape of feature B, which is located in the low-energy XANES range (see Movie 1). This result differs from what has been found in other ionic aqueous solutions in which XANES features at energy higher than 25 eV above the edge are more sensitive to structural disorder.[42] We may attribute the difference to the instable nature of the $[AuCl_4]^-$−H_2O_n cluster, much larger than that of metal cation−H_2O_n systems. Moreover, the different arrangements of water molecules occurring in the different configurations, together with the existence of Cl atoms, may also induce relatively large differences in multiple scattering paths that dominate features in the low-energy range of a XANES spectrum. The second component of the disorder comes from the oscillations of the $[AuCl_4]^-$ cluster and has an influence mainly on the high-energy range, i.e., mainly feature C and at higher energy. Feature C has a blue-shift when the Au−Cl bond decreases while a red-shift when the Au−Cl bond increases (see Movie 2). In fact, the distortion of the $[AuCl_4]^-$ plane and of the ∠Cl−Au−Cl angle on the XANES spectra has also been considered, observing negligible contributions. A comparison of both movies points out the origin of structural disorder is mainly the surrounding water molecules, while the contribution of the $[AuCl_4]^-$ cluster is relatively small.

As discussed above, structural disorder has a non-negligible effect on the spectra, therefore, it should be considered in a XANES spectrum. To this purpose, we carried out calculations starting from instantaneous configurations obtained from the MD simulation without any additional minimization. In this framework, we considered also the second hydration shell, i.e., we included all water molecules up to the distance of 5.6 Å. The corresponding summed and averaged XANES calculated from 400 MD snapshots, i.e., 400 13-hydrated configurations and 400 14-hydrated configurations are shown in Figure 8b. Clear differences are evident between the two averaged spectra: in the averaged spectrum of 14-hydrated complexes, the WL intensity is weaker, and the energy position of feature C (11 974 eV) is shifted to higher energy with respect to the experimental data (11 972 eV), while in 13-hydrated complexes, the WL intensity is stronger, and feature C appears at lower energy (11 969 eV). Moreover, it is noted that feature C also shifts to higher energy as compared with the counterpart in the spectra obtained from energy-minimization configurations, especially in the 14-hydrated species, this difference can be attributed to the exclusion of the second hydrated shell during the geometry optimization, which may have a contribution to the XANES signal.[42]

As pointed out above, the main aim of our XANES analysis is to evaluate the ratio of the hydration complexes in solution. We then carried out a linear fit with ratios $n/100$ and $(1 - n/100)$ for the 13- and the 14-hydrated complexes, respectively, and introduced the R_{sq} parameter to evaluate the goodness of fit

$$R_{sq} = \sqrt{\sum_{i \in N} (y_i^{theory} - y_i^{exp})^2}$$

here, y_i^{theory} and y_i^{exp} represent the absorption intensity of theoretical and experimental spectra at the i point, respectively. The behavior of R_{sq} vs the percentage content of the 13-hydrated complexes and averaged XANES theoretical spectra calculated with different amounts of the two coordinated species is shown in Figure 8. It shows that the best combination contains 56% and 44% of the 13- and 14-hydrated complexes, respectively. The best fit results as well as experimental data are shown in Figure 9; it is noted that some spectral features such as feature B (ranging from 11 926 to 11 938 eV) as well as a small bump between 11 946 and 11 959 eV have not been well reproduced by our theoretical scheme. We should highlight that there are no parameter optimizations in our theoretical calculation. The muffin-tin approximation used in our calculation scheme may induce some errors, which influence the spectral features in the near edge region, e.g., feature B.[43] The convolution function may affect the small bump between 11 946 and 11 959 eV. Finally, during our XANES simulations,

dx.doi.org/10.1021/jp3026623 | J. Phys. Chem. B 2012, 116, 7866−7873

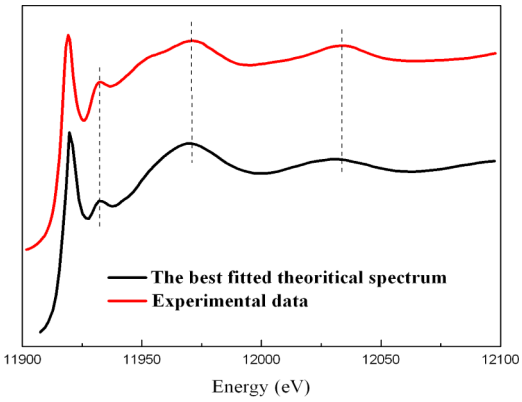

Figure 9. Best fit calculated spectrum compared with the experimental data.

we have not considered other minority components including 11-, 12-, and 15-coordinated species, while these components do have a contribution to the experimental spectrum and could be another source of discrepancy between our reproduced XANES and experimental data. Nevertheless, generally speaking, the present best fit result is in a good agreement with the experimental one. This result supports the reliability of the proposed combination of the MD simulation and MS XAS calculations to determine the content of different hydrated complexes in this aqueous solution and possibly in other aqua-complexes.

4. CONCLUSIONS

This work demonstrates that the combination of the MD simulation and XAS may provide a new and accurate structural tool to describe the local geometry of metal complexes in solution and similar liquid systems. Indeed, XAS and, in particular, the XANES method are really powerful and almost unique methods for a quantitative and reliable analysis of the short- and medium-range distributions in complex systems even with reduced or no long-range order, and the combination of MD simulation and XAS, beyond the limits of standard XANES data analysis procedure, enables us to probe the structure distribution properties in the disordered system and provides an effective and powerful strategy to resolve the microscopic hydrated structure of complex−aqueous solutions.

In this contribution, we successfully resolved the hydrated structure distribution of the $[AuCl_4]^-$ acid aqueous solution by the combination of MD simulation and XANES analysis. This scheme points out that the $[AuCl_4]^-$ cluster has a square-planar geometry with nearest water molecules around it lying in two orthogonal quasi-elliptical curved surfaces around it. Moreover, XANES experimental data supported by simulations confirm that the geometrical arrangement of water molecules in two perpendicular elliptical planes is not stable, it mainly oscillates between two configurations characterized by 13- and 14-coordinated water molecules; the 13- and 14- coordinated species are the overwhelming majority in the first hydrated shell of $[AuCl_4]^-$, with a little higher percentage of 14-coordinated species, and other components such as 11-, 12-, and 15-coordinated species only account for a very small percentage (only about 1% in our MD simulation).

■ ASSOCIATED CONTENT

Ⓢ Supporting Information

Motivations to support the selection of CEP-121G and STO-3G basis sets in the ab initio calculations; details of the scan of the potential energy surface; determination of the atomic charge and details about the effective-pair-potential fit procedure; construction of the hard core potential for water molecules at a close distance from an Au atom; influence of different atom cavity radii and value of tesseraes on the $U_{[AuCl_4]^-–H_2O}$ during the CPCM calculation; test of the statistical significance regarding the configurations considered for XANES calculations. This material is available free of charge via the Internet at http://pubs.acs.org.

■ AUTHOR INFORMATION

Corresponding Author

*E-mail: wuzy@ustc.edu.cn (Z.W.); yiluo@ustc.edu.cn (Y.L.); chenxing@ustc.edu.cn (X.C.).

Notes

The authors declare no competing financial interest.

■ ACKNOWLEDGMENTS

We would like to thank Professor Giordano Mancini and Professor Giovanni Chillemi of CASPUR for their qualified support on PCM/CPCM. A special thank goes to Dr. Derek A. Wann of the School of Chemistry of the University of Edinburgh for his technical support and to Professor Viktor A. Sipachev of the Moscow State University for the software "shrink". A sincere acknowledgement is due to Gao Bin, Zhang Qiong, and Xiu Peng for many helpful discussions, and a special thanks to Youli Hong and Haiming Li for their precious support on the software packages. This work was partly supported by the Knowledge Innovation Program of the Chinese Academy of Sciences (KJCX2-YW-N42), the Key Important Project of the National Natural Science Foundation of China (10734070), the National Natural Science Foundation of China (NSFC 11079031, 10805055, and 10905067), and the National Basic Research Program of China (2009CB930804).

■ REFERENCES

(1) Schardein, G.; Donev, E. U.; Hastings, J. T. *Nanotechnology* **2011**, *22*, 1−6.
(2) Shiying, H.; Zhirui, G.; Yu, Z.; Song, Z.; Jing, W.; Ning, G. *Mater. Lett.* **2007**, *61*, 3984−3987.
(3) Xi, L.; Zhou, J. W.; Chang, J. L. *Nanoscale Res. Lett.* **2010**, *5*, 124−129.
(4) Zhong, C. J.; Maye, M. M. *Adv. Mater.* **2001**, *13*, 1507−1511.
(5) Yeong, D. P.; Jung, A. L.; Donghoon, K.; Jeong, H. C.; Kilwon, C. *Electrochem. Solid-State Lett.* **2009**, *12*, H312−H314.
(6) Kate, B.; Muthupandian, A.; Rachel, A.; Franz, G. *J. Phys. Chem. B* **1999**, *103*, 9231−9236.
(7) Faeges, F.; Sharps, J. A.; Brown, G. E. *Geochim. Cosmochim. Acta* **1993**, *57*, 1243−1252.
(8) Chen, X.; Chu, W. S.; Chen, D. L.; Wu, Z. H.; Marcelli, A.; Wu, Z. Y. *Chem. Geol.* **2009**, *268*, 74−80.
(9) Pan, P.; Wood, S. *Geochim. Cosmochim. Acta* **1991**, *55*, 2365−2371.
(10) Pacławski, K.; Borowiec, M.; Kapusta, C.; Fitzner, K. *J. Phys. Chem. A* **2010**, *114*, 11943−11947.
(11) Jalilehvand, F.; Lindqvist-Reis, P.; Hermansson, K. *J. Am. Chem. Soc.* **2001**, *123*, 431−441.
(12) Armunanto, R.; Schwenk, C. F.; Tran, H. T.; Rode, B. M. *J. Am. Chem. Soc.* **2004**, *126*, 2582−2587.

(13) Christian, F.; Schwenk, B. M. *Chem. Phys. Phys. Chem* **2003**, *5*, 342−350.
(14) Paola, A.; Valentina, M.; Giordano, M.; Giovanni, C. *J. Phys. Chem. A* **2008**, *112*, 11833−11841.
(15) Giordano, M.; Nico, S.; Vincenzo, B.; Valentina, M.; Paola, A.; Giovanni, C. *J. Phys. Chem. B* **2008**, *112*, 4694−4702.
(16) Paola, A.; Stefano, D. L.; Alessandro, A.; Massimiliano, A.; Alfredo, D. N.; Giovanni, C. *J. Am. Chem. Soc.* **2010**, *132*, 14901−14909.
(17) Ankudinov, A. L.; Ravel, B.; Rehr, J. J.; Conradson, S. D. *Phys. Rev. B* **1998**, *58*, 7565−7576.
(18) Berendsen, H. J. C. *Comput. Phys. Commun.* **1995**, *95*, 43−56.
(19) Berendsen, H. J. C.; Postma, J. P. M.; Di, N. A.; Haak, J. R. *J. Comput. Phys* **1984**, *81*, 3684−3690.
(20) Darden, T.; York, D.; Pedersen, L. *J. Chem. Phys.* **1993**, *98*, 10089−10092.
(21) Essmann, U.; Perera, L.; Berkowitz, M. L.; Darden, T.; Lee, H.; Pedersen, L. G. *J. Chem. Phys.* **1995**, *103*, 8577−8593.
(22) Hummer, G.; Pratt, L. R.; Garcia, A. E. *J. Phys. Chem. A* **1998**, *102*, 7885−7895.
(23) Giovanni, C.; Paola, A.; Nicolae, V. P.; Nico, S.; Vincenzo, B. *J. Am. Chem. Soc.* **2002**, *124*, 1968−1976.
(24) Giovanni, C.; Vincenzo, B.; Paola, A.; Giordano, M.; Ingmar, P.; Nico, S. *J. Phys. Chem. B* **2005**, *109*, 9186−9193.
(25) Giordano, M.; Nico, S.; Vincenzo, B.; Valentina, M.; Paola, A.; Giovanni, C. *J. Phys. Chem. B* **2008**, *112*, 4694−4702.
(26) McWeeny, R.; Dierksen, G. *J. Chem. Phys.* **1968**, *49*, 4852−4862.
(27) Hay, P. J.; Wadt, W. R. *J. Chem. Phys.* **1985**, *82*, 270−283.
(28) Wadt, W. R.; Hay, P. J. *J. Chem. Phys.* **1985**, *82*, 284−298.
(29) Hay, P. J.; Wadt, W. R. *J. Chem. Phys.* **1985**, *82*, 299−310.
(30) Hehre, W. J.; Stewart, R. F.; Pople, J. A. *J. Chem. Phys.* **1969**, *51*, 2657−2664.
(31) Collins, J. B.; Schleyer, P. V. R.; Binkley, J. S.; Pople, J. A. *J. Chem. Phys.* **1976**, *64*, 5142−5151.
(32) Kendall, R. A.; Harrison, R. J. *J. Chem. Phys.* **1992**, *96*, 6796−6806.
(33) Foresman, J. B.; Frisch, Æ. *Exploring Chemistry with Electronic Structure Methods*, 2nd ed.; Gaussian Inc.: Pittsburgh, PA, 1996.
(34) Giovanni, C.; Giordano, M.; Nico, S.; Vincenzo, B.; Stefano, D. L.; Maurizio, B.; Nicolae, V. P.; Paola, A. *J. Am. Chem. Soc.* **2007**, *129*, 5430−5436.
(35) Paola, A.; Valentina, M.; Giordano, M.; Giovanni, C. *J. Phys. Chem. A* **2008**, *112*, 11833−11841.
(36) Paola, A.; Barone, V.; Chillemi, G.; Sanna, N.; Meyer-Klaucke, W.; Pavel, N. V. *J. Am. Chem. Soc.* **2002**, *124*, 1968−1976.
(37) Hoffmann, M. M.; Darab, J. G.; Palmer, B. J.; Fulton, J. L.; Reeder, R. J. *J. Phys. Chem.* **1999**, *103*, 8471−8482.
(38) Elzinga, E. J.; Reeder, R. J. *Geochim. Cosmochim. Acta* **2002**, *66*, 3943−3954.
(39) Stillinger, F. H.; Rahman, A. *J. Chem. Phys.* **1974**, *60*, 1545−1557.
(40) Head-Gordon, T.; Stillinger, F. H. *J. Chem. Phys.* **1993**, *98*, 3313−3327.
(41) Mahoney, W.; Jorgensen, W. L. *J. Chem. Phys.* **2000**, *112*, 8910−8922.
(42) Paola, A.; Roscioni, O. M.; Chillemi, G.; Della, L. S.; Benfatto, M. *J. Am. Chem. Soc.* **2006**, *128*, 1853−1858.
(43) Rehr, J. J.; Albers, R. C. *Rev. Mod. Phys.* **2000**, *72*, 621−654.